Passive and Active Flow Control by Swimming Fishes and Mammals

F.E. Fish[1] and G.V. Lauder[2]

[1]Department of Biology, West Chester University, West Chester, Pennsylvania 19383; email: ffish@wcupa.edu

[2]Museum of Comparative Zoology, Harvard University, Cambridge, Massachusetts 02138; email: Glauder@oeb.harvard.edu

Annu. Rev. Fluid Mech. 2006. 38:193–224

The *Annual Review of Fluid Mechanics* is online at fluid.annualreviews.org

doi: 10.1146/annurev.fluid.38.050304.092201

0066-4189/06/0115-0193$20.00

Key Words

vorticity, locomotion, tubercles, digital particle image velocimetry, flukes, biomechanics, hydrodynamics, biomimetic

Abstract

What mechanisms of flow control do animals use to enhance hydrodynamic performance? Animals are capable of manipulating flow around the body and appendages both passively and actively. Passive mechanisms rely on structural and morphological components of the body (i.e., humpback whale tubercles, riblets). Active flow control mechanisms use appendage or body musculature to directly generate wake flow structures or stiffen fins against external hydrodynamic loads. Fish can actively control fin curvature, displacement, and area. The vortex wake shed by the tail differs between eel-like fishes and fishes with a discrete narrowing of the body in front of the tail, and three-dimensional effects may play a major role in determining wake structure in most fishes.

1. INTRODUCTION

Aquatic animals have evolved a diversity of propulsive mechanisms to locomote effectively through water. These mechanisms are a result of a long evolutionary history during which selection has acted on propulsive systems and generated an array of novel anatomical and physiological responses to the problem of moving though water (Fish 2000, Lauder & Drucker 2004). Aquatic animals (e.g., fishes, whales, seals, penguins) produce hydrodynamic thrust by acceleration of water through movement of their body and appendages, while simultaneously reducing the resistance to their motion through morphological design, phased kinematics, and behaviors.

Interest in animal hydrodynamics is related largely to flow control. Animals have been hypothesized to control flow both passively and actively, effecting enhanced performance in drag reduction, thrust production, and propulsive efficiency. Passive control is related to the anatomy of the animal, with morphology and structural features dictating flow over the animal's surface. Controlling flow regimes within the boundary layer has been at the center of long-standing arguments related to the possibility that animals use clever drag reduction mechanisms (Anderson et al. 2001, Gray 1968). In active control, the movements of the animal, under active muscular control, modify flow directly. Vorticity shed from the body or fins as structured vortices or shear layers is utilized to vector hydrodynamic forces during propulsion, maneuvering, and trim control.

This paper is not a comprehensive review of all aspects of aquatic locomotion in fishes and mammals, a topic far too diverse to cover in a meaningful manner here; a number of recent works provide overviews of much relevant biological and hydrodynamic literature (Bandyopadhyay 2004; Fish 2004; Lauder 2005; Lauder & Drucker 2004; Triantafyllou et al. 2000, 2004; Webb 1998; Wilga & Lauder 2004a). This discussion focuses on mechanisms of biological flow control by aquatic fishes and mammals, a topic with both a long history and considerable new data that reflect growing interest in understanding how organisms control fluid flow around their bodies and appendages.

2. PASSIVE FLOW CONTROL

2.1. Gray's Paradox

One of the most hotly debated ideas within biofluiddynamics has been the mechanism of viscous dampening for passive flow control to reduce drag in dolphins. The controversy known as "Gray's Paradox" resulted from the first attempt to evaluate swimming energetics through a simple hydrodynamic model (Fish & Hui 1991, Gray 1936, Webb 1975). A rigid-body hydrodynamic model was used to calculate drag power of a dolphin and a porpoise swimming at high speeds (>7.6 m/s; Reynolds number $>10^6$). The results indicated that the estimated drag power could not be reconciled with the available power generated by the muscles (Gray 1936).

Gray's (1936) calculations assumed that turbulent flow conditions existed in the boundary layer. His resolution to the problem was that the fully laminar boundary

layer was maintained despite accepted hydrodynamic theory. The assertion that dolphins could maintain a laminar boundary layer remained and became the focus and justification of much of the work on dolphin hydrodynamics for the next 60 years (Fish & Hui 1991, Fish & Rohr 1999, Lang & Daybell 1963, Romanenko 1995).

The basic premise of Gray's Paradox, however, was flawed because of potential errors in estimation of dolphin swimming speed and inconsistencies between dolphin swimming performance and data on muscle power outputs. Gray used an observation of a dolphin swimming along the side of the ship from stern to bow in 7 seconds. If the dolphin was swimming close enough to utilize the flow pattern around the ship, its speed may have been artificially enhanced and energetic effort reduced due to the pressure distribution close to the ship (Lang 1966, Weihs 2004, Williams et al. 1992). In addition, the duration of this high-performance swimming was for a sprint and Gray used measurements for muscle power output of sustained performance (3–5 minutes) by human oarsmen (Henderson & Haggard 1925). Muscle fibers specialized for quick bursts can produce power outputs 2–17 times greater than muscle fibers used for sustained activities (Askew & Marsh 1997).

Dolphins have the muscular capacity to swim at high speeds for short durations while maintaining a fully attached turbulent boundary layer. The turbulent flow conditions would delay separation of the boundary layer (**Figure 1**; Rohr et al. 1998). When the boundary layer separates from the skin surface and interacts with outer flow, this results in a broader wake and increased drag, so delaying separation is beneficial to the dolphin. Separation is more likely to occur with a laminar boundary flow, producing a greater drag penalty compared to turbulent boundary conditions. Thus, the turbulent boundary layer remains attached longer because it has more energy than the laminar boundary layer. The increased drag of a turbulent boundary layer

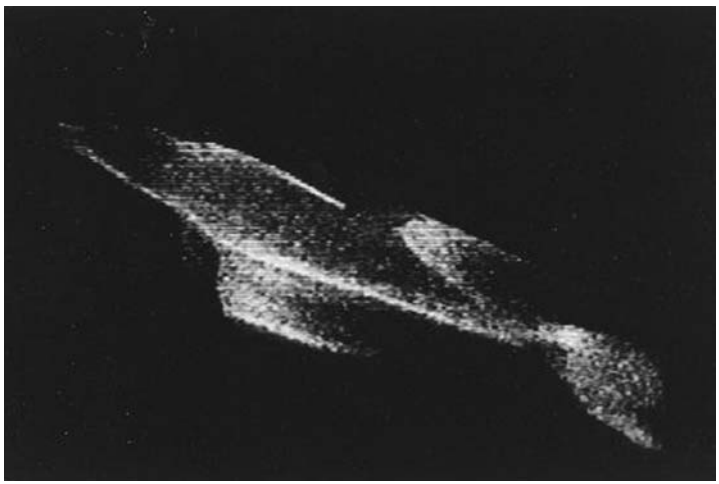

Figure 1

Bioluminescence image of gliding dolphin. Courtesy of J. Rohr.

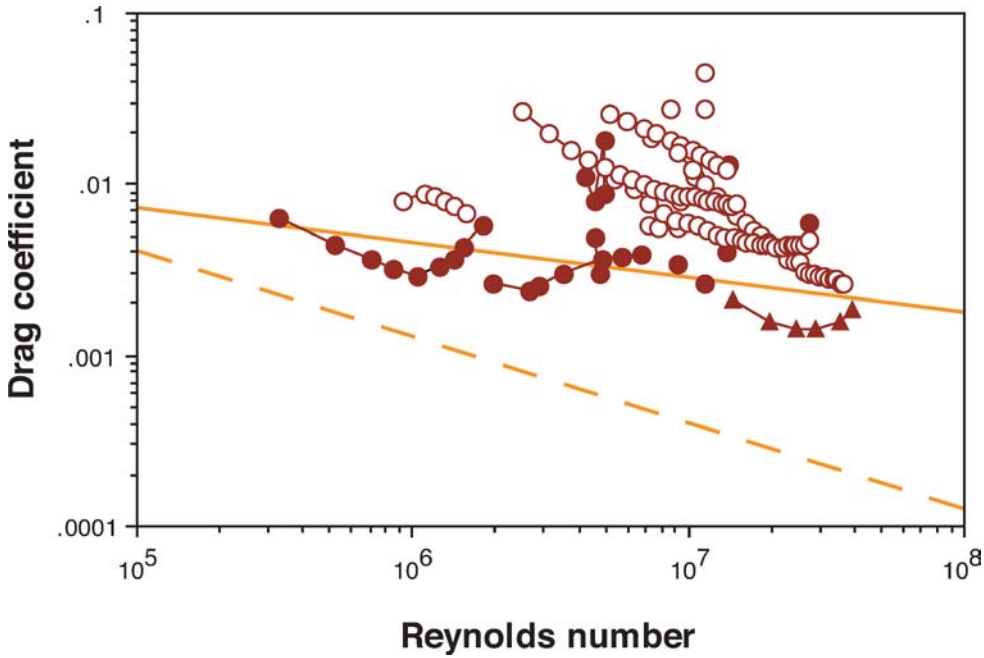

Figure 2

Drag coefficient plotted against Reynolds number for cetaceans. Data were obtained from experiments on rigid models, towed bodies, and gliding animals (*closed circles*) and from hydrodynamic models based on swimming kinematics (*open circles*). The upper solid line represents the drag coefficient for a flat plate with turbulent boundary layer and the lower dashed line is for a flat plate with laminar boundary flow. Solid triangles are drag coefficients for a rigid solid of revolution of the NACA 66 series. Figure from Fish & Rohr (1999).

is small compared to the increase in drag due to separation, which is more prone to occur with a laminar boundary layer. When dolphins were actively swimming, flow separation appeared to be restricted to the tips of the lifting surfaces (i.e., flukes, flippers, and dorsal fin) (Wood 1973).

Drag coefficients (C_D) for dolphins indicated full turbulent or transitional boundary layers (Fish & Rohr 1999; **Figure 2**). In general, data obtained from hydrodynamic models of actively swimming animals are higher than values from towing or gliding experiments and higher than theoretical frictional drag coefficients with turbulent boundary conditions (Fish 1998b). Studies using towed models and gliding dolphins gave mixed results with some values of C_D below fully turbulent conditions (Kayan 1974). However, as Reynolds number (Re) increased, C_D climbed into the turbulent regime (**Figure 2**). No difference in drag was apparent when tripping rings were carried by a dolphin during gliding experiments (Lang & Daybell 1963).

For actively swimming dolphins, high C_D is expected because the oscillating motions of the flukes and body will produce boundary layer thinning (Lighthill 1971).

The increased drag corresponds to a boundary layer that is thinner than that for a rigid body due to movements of the body perpendicular to the boundary flow. Lighthill (1971) estimated that skin friction could increase up to a factor of five. This effect was confirmed using computational fluid dynamics for undulatory swimming (Liu et al. 1997), and also by Anderson et al. (2001) in experimental studies of swimming fish boundary layers. In addition, the pressure component of drag increases because the propulsive motions of the body produce a deviation from a streamlined body (Fish 1993, Fish et al. 1988). Behavioral patterns by diving mammals and birds demonstrate energetic savings by passive gliding (Williams et al. 2000).

The idea that laminar flow could be maintained over the entire body of the dolphin was invigorated by Kramer (1960a, 1960b). Kramer claimed that the dolphin's smooth, compliant skin could achieve a laminar boundary layer without separation. The skin was proposed to deform and eliminate drag by viscous dampening. In viscous dampening, the compliance of the skin due to its viscoelastic properties would absorb energy from pressure oscillations and dampen perturbations of the Tollmien-Schlichting wave type to maintain laminar flow. A torpedo with an artificial skin based on the skin of a dolphin reportedly produced a 59% reduction in drag when compared to a reference model with fully turbulent flow. Attempts to later verify Kramer's results on passive compliance subsequently failed (Landahl 1962, Riley et al. 1988), although some limited success in reducing skin friction has been possible with other compliant coatings (Carpenter 2000, Gad-el-Hak 1987).

Other possible mechanisms for drag reduction have focused on active skin compliance by large mobile skin folds (Aleyev 1977, Nagamine et al. 2004, Sokolov et al. 1969), addition of non-Newtonian additives from skin sloughing (Harrison & Thurley 1972, Nagamine et al. 2004), matching shear impedance of a developing turbulent boundary layer to the dolphin's blubber (Fitzgerald et al. 1995), secretions from the dolphin eye (Sokolov et al. 1969, Uskova et al. 1983), viscosity reduction by boundary layer heating (Fish & Hui 1991, Lang 1966, Lang & Daybell 1963), accelerated water flow due to propulsive movements of the caudal flukes (Gray 1936, Romanenko 1995), and muscular control by microvibrations (Haider & Lindsley 1964, Ridgway & Carder 1993). However, these mechanisms provided no drag reduction for dolphins (Fish 1998b, Fish & Hui 1991, Fish & Rohr 1999, Rohr et al. 1998, Webb 1975).

2.2. Leading Edge Tubercles

The humpback whale flipper is unique because of the presence of large, rounded protuberances or tubercles located on the leading edge, which give this surface a scalloped appearance (**Figure 3**; Fish & Battle 1995). The position and number of tubercles on the flipper suggested analogues with specialized leading edge control devices associated with improvements in hydrodynamic performance (Fish & Battle 1995, Miklosovic et al. 2004). Bushnell & Moore (1991) suggested that humpback tubercles may reduce drag due to lift on the flipper.

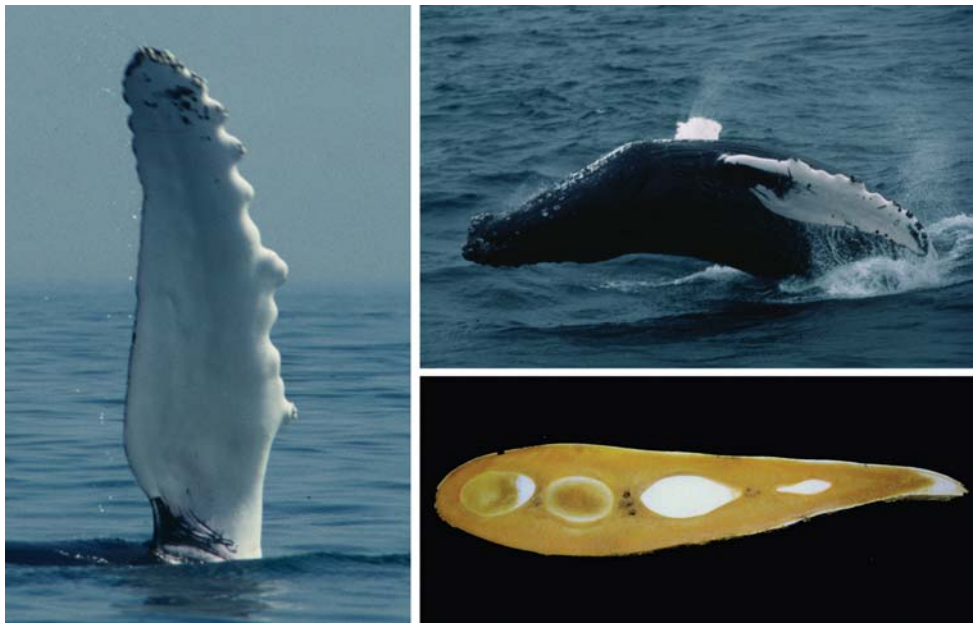

Figure 3

Humpback whale (*Megaptera novaeangliae*) flipper: leading edge tubercles (*left*), breaching humpback whale showing relative size of the flipper (*top right*), and cross section of flipper (*bottom right*). Photographs of whale courtesy of W.W. Rossiter.

The occurrence of "morphological complexities" on a lifting body could reduce, or use, pressure variation at the tip to decrease drag and improve lift to prevent tip stall. Alternatively, various biological wings utilize leading edge control devices to maintain lift and avoid stall at high attack angles and low speeds. Lifting bodies used in turning must operate at high angles of attack while maintaining lift (Weihs 1993). Humpback whale flippers are used in tight turning maneuvers associated with the whale's feeding ecology (Fish & Battle 1995). The tubercles of the humpback whale flipper may function to generate vortices by excitation of flow to maintain lift and prevent stall at high angles of attack.

Experiments on wavy bluff bodies showed periodic variation in the wake width across the span (Owen et al. 2000), which resulted in a drag reduction of at least 30% compared to equivalent straight bodies (Bearman & Owen 1998). Wind tunnel experiments using humpback whale flipper models provided evidence that the leading edge tubercles serve to delay stall angle and increase total lift without increasing drag (Miklosovic et al. 2004). Stall angles occurred at 12° and 16.3° for the models without and with tubercles, respectively (**Figure 4*a***). The maximum lift was somewhat greater for the model flipper with tubercles (**Figure 4*a***). The drag coefficient for the model with tubercles was less than without tubercles in the range $12° < \alpha < 17°$ and was only slightly greater in the range $10° < \alpha < 12°$. (**Figure 4*b***). Peak lift/drag was greater when tubercles were present (**Figure 4*c***).

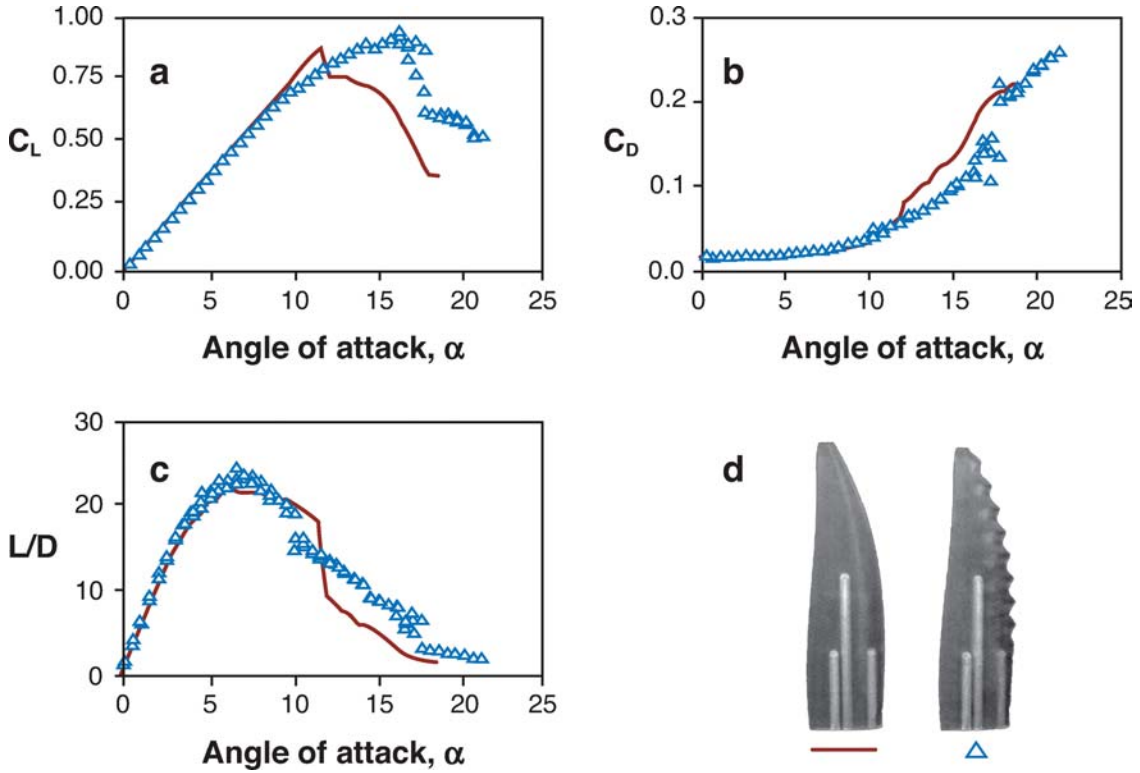

Figure 4

Lift and drag data for humpback whale flipper models, with and without tubercles. The solid lines in *a*, *b*, and *c* show the average of the data for the flipper model without tubercles. Triangles indicate data for flipper with tubercles. Wind tunnel measurements of (*a*) lift coefficient, C_L, (*b*) drag coefficient, C_D, and (*c*) aerodynamic efficiency, L/D, displayed as a function of angle of attack, α. (*d*) Model with and without tubercles. From Miklosovic et al. (2004).

A panel method simulation for wing sections with leading edge tubercles at a 10° angle of attack (**Figure 5**) demonstrated a 4.8% increase in lift, a 10.9% reduction in induced drag, and a 17.6% increase in lift to drag ratio in comparison to wings without tubercles (Watts & Fish 2001). Tubercles enhanced flipper performance at modest angles of attack while offering no detrimental effects at zero angle of attack. Unsteady Reynolds-averaged Navier-Stokes (RANS) simulation (Paterson et al. 2003) on a NACA 63–021 baseline foil with and without equally spaced tubercles showed flow separation patterns and surface pressure were dramatically altered by the tubercles (**Figure 6**). For regions downstream of the tubercle crest, separation was delayed almost to the trailing edge. This appears to be due to an increase in pressure on the suction side, which locally reduces the adverse pressure gradient. The tubercles generate chordwise vorticity in the troughs as flow is convected along the leading edge (**Figure 6**). In addition, the flow directly over the tubercle

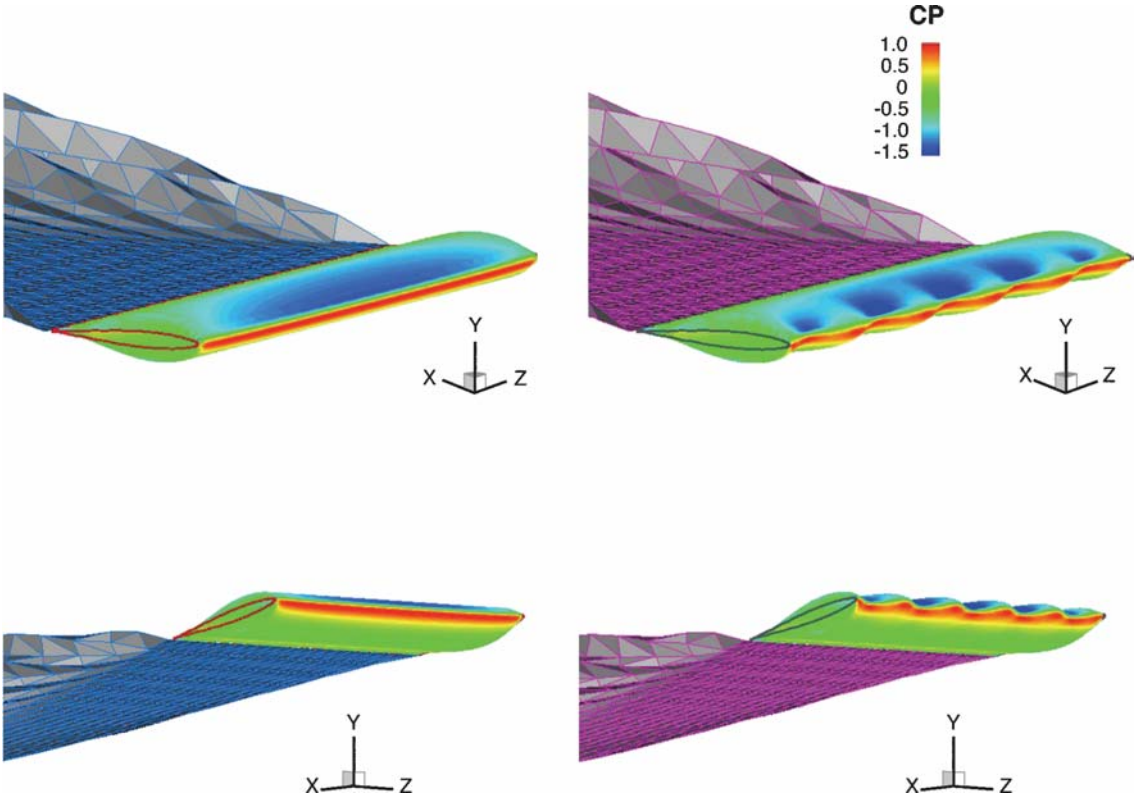

Figure 5

Panel method simulation of flow over an finite span wing at $\alpha = 10^\circ$ with straight leading edge (*left*) and leading edge tubercles (*right*) with top (*upper*) and bottom (*lower*) views. Colors represent the pressure differences on the wing. From Watts & Fish (2003).

is accelerated posteriorly. These effects push the stall line further posterior on the flipper.

Modification of the leading edge to control flow around a lifting surface are also observed in sharks. Hammerhead sharks have large leading protuberances on their cephalofoil (head), which could control flow and reduce drag due to lift (Bushnell & Moore 1991). Large scales (dermal denticles) have been found along the elongate pectoral fins of fossil chondrichthyans (Zangerl & Case 1973). Such structures may energize the boundary layer and prevent separation and stall.

2.3. Dermal Denticles as Riblets

The use of riblets to reduce turbulent skin friction came in part from the study of modern shark dermal denticles (Walsh 1990). Riblets are streamwise microgrooves that act as fences to break up spanwise vortices and reduce the surface shear stress

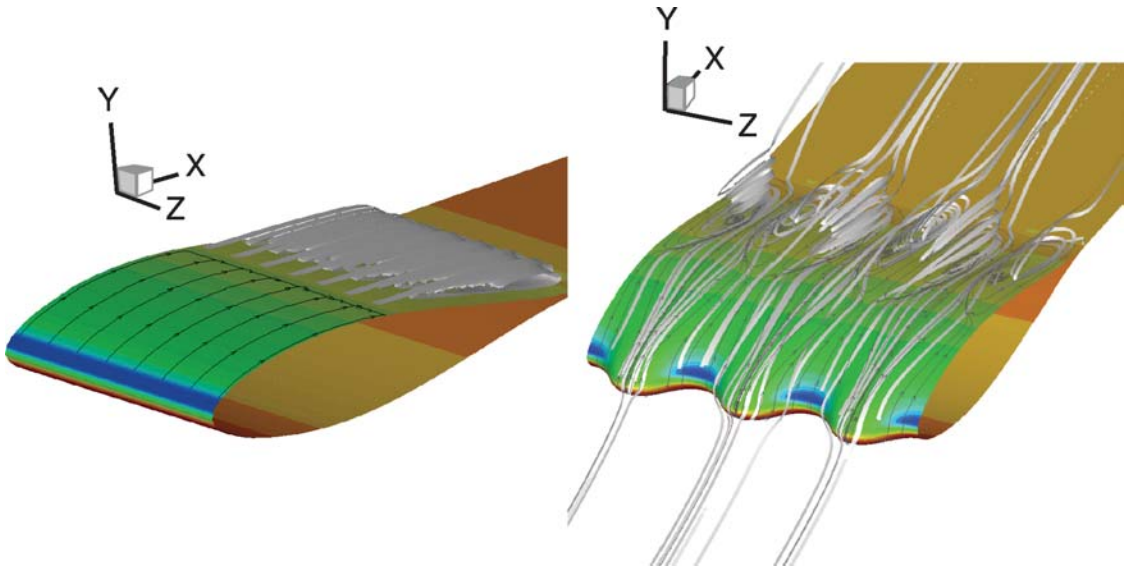

Figure 6

Pressure contours and streamlines at $\alpha = 10^{\circ}$ for NACA 63–021 with straight leading edge (*left*) and with tubercles (*right*). An unsteady Reynolds-averaged Navier-Stokes (RANS) simulation was used. A separation line is shown on the wing section without tubercles. For the wing with tubercles, large vortices are formed posterior of the troughs along the leading edge and flow posterior of the tubercles is shown as straight streamlines without separation. Images courtesy of E. Paterson.

and momentum loss by preventing eddies from transporting high speed fluid close to the surface (Choi et al. 1993; Moin & Kim 1997). Fast-swimming sharks have scales with flat crowns and sharp ridges that are oriented longitudinally with rounded valleys (Reif 1978, Reif & Dinelacker 1982). Although the ridges are discontinuous due to the distribution of the scales, a 7–8% drag reduction is possible and values in this range have been measured for continuous riblets (Walsh 1990). The streamwise surface grooves of scallop shells also indicate that these organisms use riblets (Anderson et al. 1997). Optimal riblet spacing is present in those scallops demonstrating the greatest swimming ability. Small ridges on the epidermis of dolphins had been hypothesized to stabilize longitudinal vortices (Yurchenko & Babenko 1980), but the geometry of the ridges with rounded edges does not suggest an effective analogy with riblets (Fish & Hui 1991).

3. ACTIVE FLOW CONTROL

3.1. Demonstrating Active Flow Control

Hydrodynamic forces acting on a flexible body and appendages could produce motion that appears to be generated by the animal, when in fact the observed movements are

passive. It is all too easy to observe vortical structures in the wake shed by fins, flukes, or the moving body and conclude that these flow structures are actively generated. But a variety of flow patterns could result from the passive interaction of an appendage and the fluid.

With fish fins, demonstrating active flow control is particularly difficult as fins are highly flexible structures easily deformed by imposed fluid loads. Extreme bending of fish fins can be observed during rapid movements (e.g., Jayne et al. 1996), and the relative contribution of active and passive deformation remains unclear for the vast majority of cases studied. Also, as swimming animals change speed, the relative contributions of active and passive effects may change (Lauder & Drucker 2004).

3.2. Vorticity Production by the Body and Tail

The recent availability to biologists of high-speed video cameras (with frame rates of 250 to 2000 fps and greater) that can obtain high-resolution images (1024 by 1024 pixels or greater at these higher frame rates), coupled with continuous wave lasers of moderate power (10 W), has allowed a number of detailed studies of fluid flows produced by swimming animals using digital particle image velocimetry (DPIV; e.g., Drucker & Lauder 1999, 2002b; Lauder & Drucker 2002; Lauder et al. 2003; Nauen & Lauder 2001a; Wilga & Lauder 2004b; Wolfgang et al. 1999). Using high-speed cameras and continuous wave lasers permits excellent time resolution of vorticity generation as the body and appendages of swimming animals move; using pulsed laser systems typically provides poor temporal sampling for most biological movements in the 1–100-Hz range. Unsteady maneuvering movements in particular require continuous recording of flow fields at a rate of at least 250 Hz.

Although the body and tail in fishes are often treated together as a single flexible, undulating foil (Muller et al. 1997), we caution that kinematic studies have shown that the tail of fishes may undergo complex deformations independent of the body (Ferry & Lauder 1996, Gibb et al. 1999, Lauder 2000). Fish tails have considerable intrinsic musculature (Gibb et al. 1999, Lauder 1982, Winterbottom 1974) that enables fishes to alter tail camber, area, and angle of attack during the tail beat (Lauder 2000, Lauder et al. 2003), thus shedding vorticity in unexpected ways. It is demonstrably not true that the tail of most fishes functions simply as a passive extension of the body when viewed in three dimensions. Indeed, the distinct morphological separation of the tail in most fishes via the considerable narrowing of the body at the region just in front of the tail (**Figure 7*a***) suggests that most fish tails function as a distinct propeller, largely independent from the major drag-incurring body region anteriorly (Nauen & Lauder 2000, 2001b). Scombrid fishes (e.g., mackerel, tuna) also possess an array of distinct finlets, small separate fins, along the upper and lower margins of the caudal peduncle region. Finlet kinematic and flow patterns have been described by Nauen & Lauder (2000, 2001a,b).

This view of the fish tail as a propeller rather than simply a flexible extension of the body is also supported by patterns of vortex ring production by swimming fish tails. Vortex rings shed by discrete fish tails show central momentum jets oriented to the

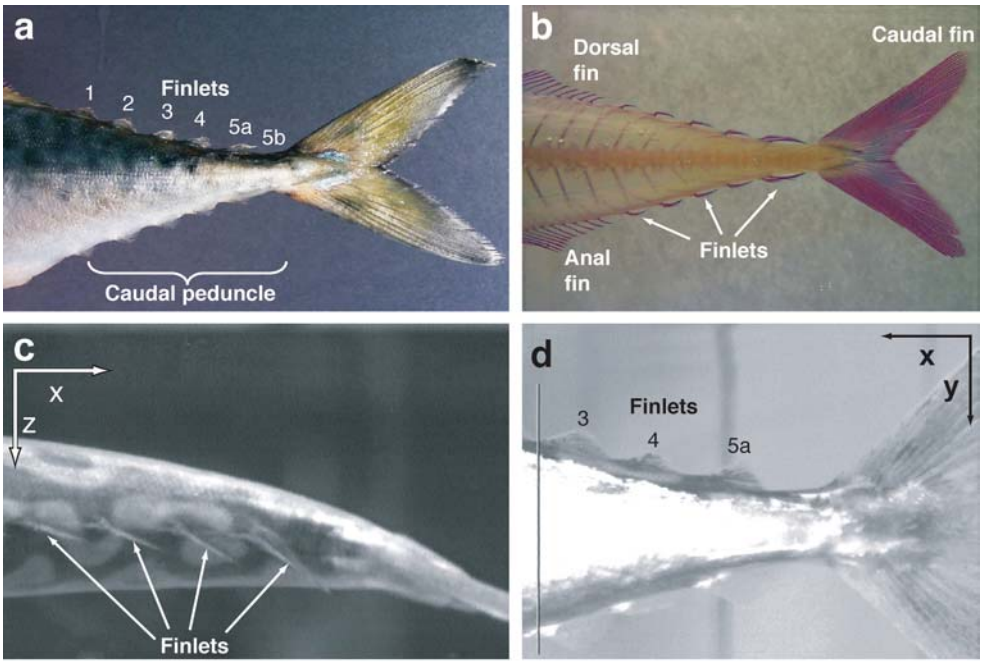

Figure 7

Tail (caudal fin) anatomy in mackerel (*Scomber japonicus*). Note the rapid narrowing of the lateral (side) body profile in front of the tail known as the caudal peduncle. (*a*) Mackerel have rows of small finlets located in front of the tail along the upper and lower body margins: These are numbered from 1 to 5, and the most posterior finlet is composed of two closely apposed finlets, which are labeled 5*a* and 5*b*. (*b*) Bones (the vertebral column and fin rays in the fins) have been stained red, and muscle tissue enzymatically removed. (*c*,*d*) Synchronous top and side views of the body, tail, and finlets during steady swimming in mackerel from high-speed video frames. Note the deflection of the finlets. (Modified from Nauen & Lauder 2000, 2001b.)

side and backward, producing a thrust signature in the wake (Lauder & Drucker 2002; Lauder et al. 2003; Muller et al. 1997; Nauen & Lauder 2002a, 2002b; Wolfgang et al. 1999). Most bony fishes possess tails with an externally symmetrical shape (**Figure 7**): These tails are termed homocercal (Gosline 1971, Lauder 1989). Ellipsoidal vortex rings (**Figure 8**) are generated as fish with homocercal tails swim and have a minor axis (height) effectively equal to tail height, and a major axis (length) determined by swimming speed. The central momentum jet through the center of each vortex ring is typically not horizontal, but is angled down due to asymmetrical motion of the upper and lower tail lobes, which direct flow slightly down (Lauder & Drucker 2002; Lauder et al. 2002, 2003). This induces torques around the center of mass that must be balanced by forces generated with other fins (Gibb et al. 1999). In addition, this momentum jet is angled back and to the side (**Figure 8*b*,*d***), indicating substantial momentum addition in the free-stream direction.

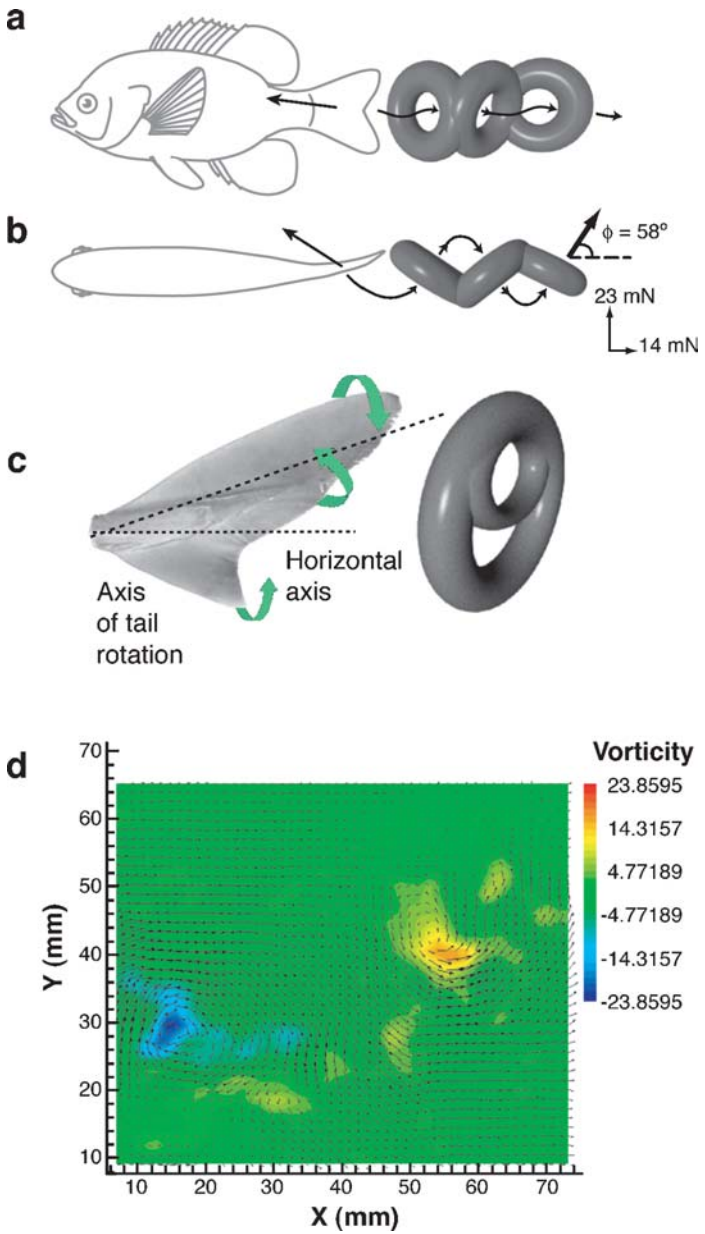

Figure 8

Vortex rings shed from fish with homocercal tails during steady swimming in side (*a*) and top (*b*) view. Mean central jet flow angle and force through tail vortex rings is shown behind the rings in b. (*c*) The ring-within-a-ring vortex wake shed from the tail of spiny dogfish sharks during steady swimming. A linked chain of vortex rings is present, but only one is shown here for clarity. (*d*) Fluid velocity and vorticity in the wake of a freely swimming trout, *Oncorhynchus mykiss*. Free-stream flow is from left to right and has been subtracted to reveal vortical structures. Note the two counter-rotating centers and the large area of higher momentum jet flow in between these centers directed to the side and downstream. (Modified from Lauder et al. 2002, Nauen & Lauder 2002a, Wilga & Lauder 2004b.)

There are few data on the hydrodynamic environment of the region just in front of the tail leading edge, but the analyses that have been done suggest that flow is strongly three-dimensional as the tail moves to the side (Nauen & Lauder 2001a).

Sharks and fishes such as sturgeon possess externally asymmetrical tails termed heterocercal (Lauder et al. 2003); the upper lobe is larger than the lower lobe, and

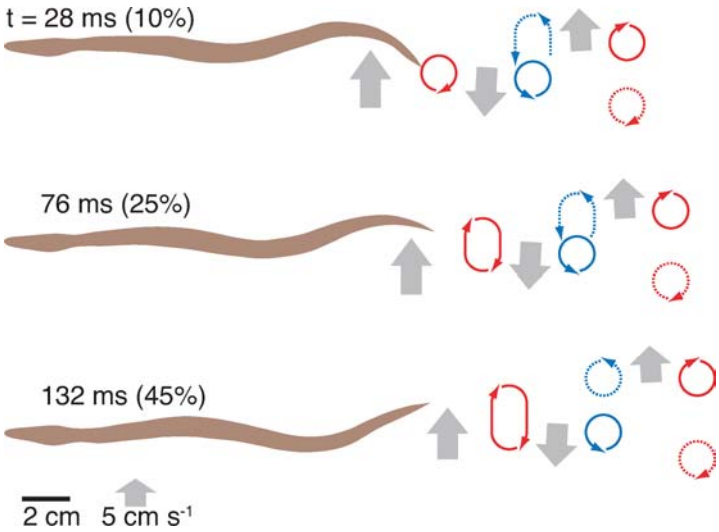

Figure 9

Schematic summary of the wake behind a steadily swimming eel at three different times in a tail beat cycle, derived from experimental hydrodynamic analysis of steadily swimming eels, *Anguilla rostrata*. Vortices are shown by red and blue curved arrows, and lateral jets are indicated by block arrows with lengths and orientation corresponding to jet flow magnitude and direction. Vortices form by the rollup of the shear layer shed by the tail. Note the relative lack of body movement in the front half of the eel. (Modified from Tytell & Lauder 2004.)

the tail possesses an inclined trailing edge (**Figure 8*c***). Vortex rings shed from the heterocercal tail of spiny dogfish sharks possess a ring-within-a-ring structure due to the temporal asymmetry in tip vortex rollup between the upper and lower tail lobes (Wilga & Lauder 2004b). Formation of the shark tail ring-within-a-ring structure vortex structure appears to occur by a similar mechanism to that of ring formation when fluid is ejected from cylinders with inclined orifices (Webster & Longmire 1997, 1998).

In fish such as eels that lack a distinct propeller-like tail region, the vortex wake has a different appearance with momentum directed almost purely sideways (Tytell 2004a, Tytell & Lauder 2004). This pattern results from formation of an unstable shear layer leaving the tail tip that rolls up into two vortices over time. **Figure 9** shows this process schematically, and **Figure 10** shows details of the rollup measured from experimental hydrodynamic analyses of eel swimming (Tytell & Lauder 2004). The resulting vortex wake consists of pairs of vortices with a central momentum jet pointing laterally, with little downstream momentum. Thus, the wake of swimming eels differs from the typical wake of fishes with discrete propeller-like tails in which there is a clear thrust signature (e.g., **Figure 8*d***). The lack of such downstream momentum in eel wakes may be a result of both a rough temporal and spatial balance of momentum addition and removal along the body, and the relatively uniform longitudinal body profile lacking major changes in area and a distinct tail.

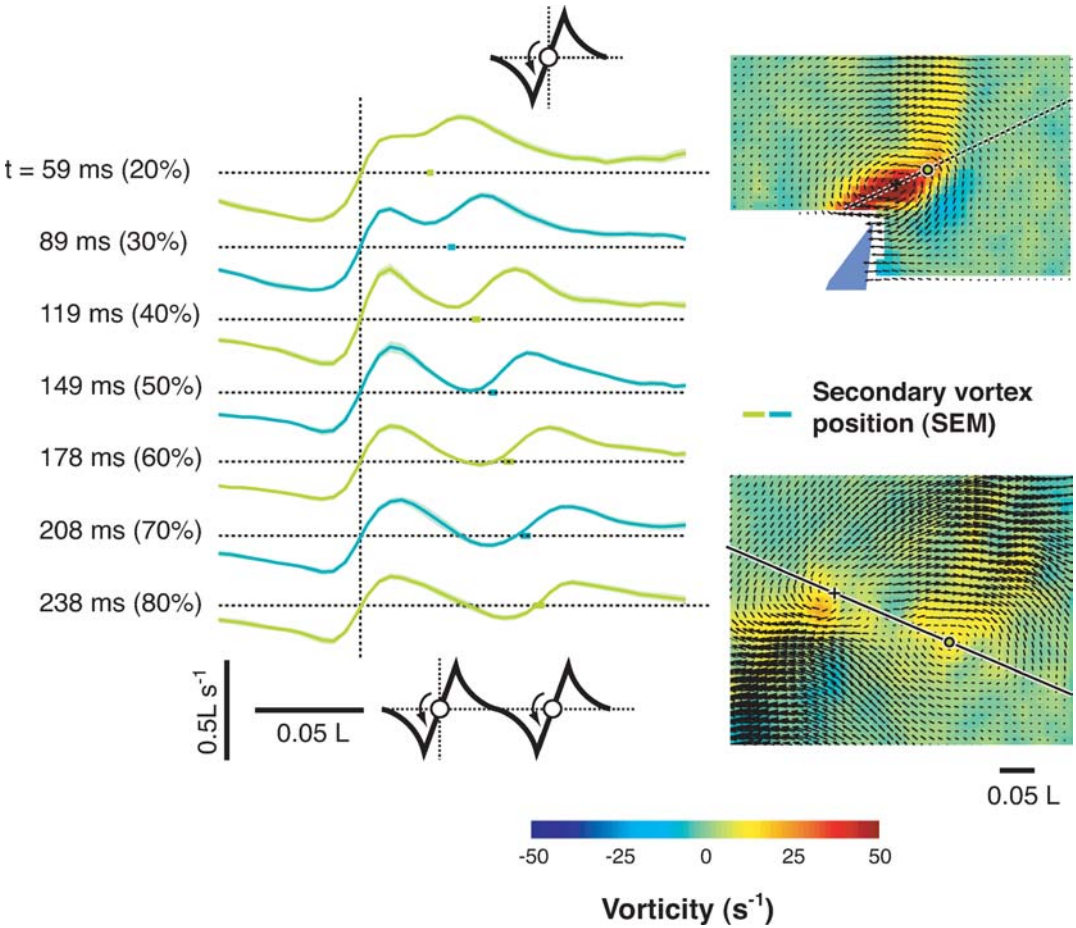

Figure 10

Velocity transects through vortices in the wake of a steadily swimming eel to show the separation through time of the two vortex cores. The location of the center of the first vortex is indicated by the vertical dotted line, and zero velocity by horizontal dotted lines at each time. Sample flow fields at the times indicated by the arrows are shown on the right. The center of the first vortex core is indicated by a cross, and the center of the second by a circle. Idealized profiles through a single and two same-sign Rankine vortices are shown above and below the transect plots, respectively. Transect plots show fluid velocity at seven points through time along the line connecting the two vortex centers as indicated on the vorticity and vector plots to the right. (Modified from Tytell & Lauder 2004.)

The front half of the body of swimming eels produces very low vorticity, consistent with observed kinematic patterns in which steadily swimming eels at low to moderate speeds of 0.5 to 1.5 Ls^{-1} possess relatively little lateral body motion in this region (Gillis 1996, 1998; Tytell 2004a; Tytell & Lauder 2004). Indeed, the view that eel locomotion involves large sideways movement of nearly the entire body even at slow

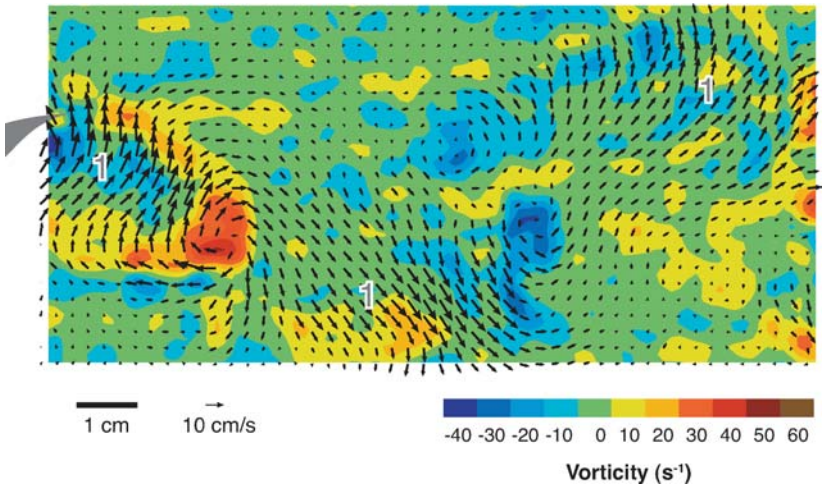

Figure 11

Vortex wake of an accelerating eel. Acceleration is toward the left at 0.6 Ls^{-2} by an eel starting from steady swimming at 1.42 Ls^{-1}. Note the strong downstream jet flows between vortex cores (labeled 1), similar in direction and relative magnitude to steady swimming in fish with distinct tail propellers. (Modified from Tytell 2004b.)

swimming speeds is one of the most enduring inaccuracies in the literature of aquatic swimming. Many workers accept the kinematic patterns shown for eels by Gray (1933) in his classic paper as a canonical representation of eel swimming. But, as discussed by Lauder & Tytell (2004), Gray's eels were small individuals that were most likely accelerating. Accelerating eels do exhibit much larger anterior side movements (Tytell 2004b). But eels swimming in a controlled steady rectilinear manner do not display this pattern, and instead exhibit an amplitude envelope that is remarkably similar to that of other fishes (Lauder 2005): very low amplitude motion in the front half of the body, and rapidly increasing amplitude in the last one third of the body.

However, during linear accelerations by eels the thrust signature of downstream momentum in the wake that is absent during steady swimming appears (**Figure 11**). Tytell (2004b) studied carefully controlled linear accelerations ranging from −1.4 to 1.3 Ls^{-2} and showed that axial fluid momentum appearing in the eel wake is significantly correlated with the magnitude of body acceleration. Thus, axial momentum in aquatic vortex wakes can reflect thrust, demonstrating the necessity of carefully controlling animal body movement and kinematic patterns when attempting to draw conclusions about the hydrodynamic structure of the wake.

The maximum spatial amplification and optimal creation of thrust-producing jet vortices lies in a narrow range of nondimensional frequencies referred to as the Strouhal number (*St*) (Triantafyllou et al. 1991). Peak swimming efficiencies for cetaceans and fish occur at $St = 0.2–0.4$ (**Figure 12**; Rohr & Fish 2004, Triantafyllou & Triantafyllou 1995). Animal propeller efficiencies have been estimated at 0.77 to 0.98 (Fish 1998b, Fish & Rohr 1999, Webb 1975).

3.3. Structure of Fish Fins

The fins of all fishes are stiffened with internal supporting elements, fin rays, that serve as sites of muscle attachment and support for the thin collagenous fin

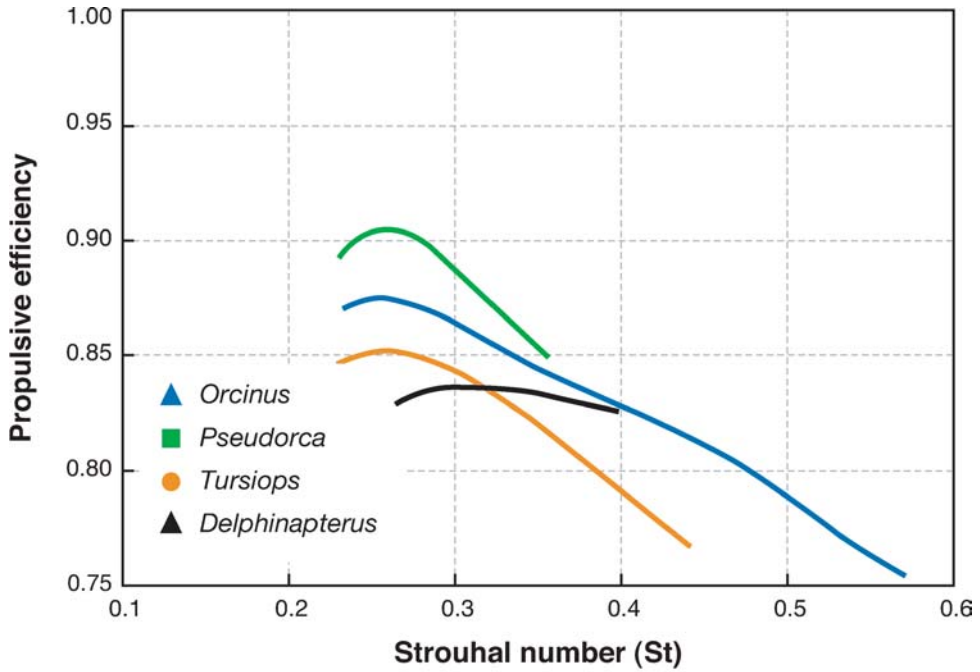

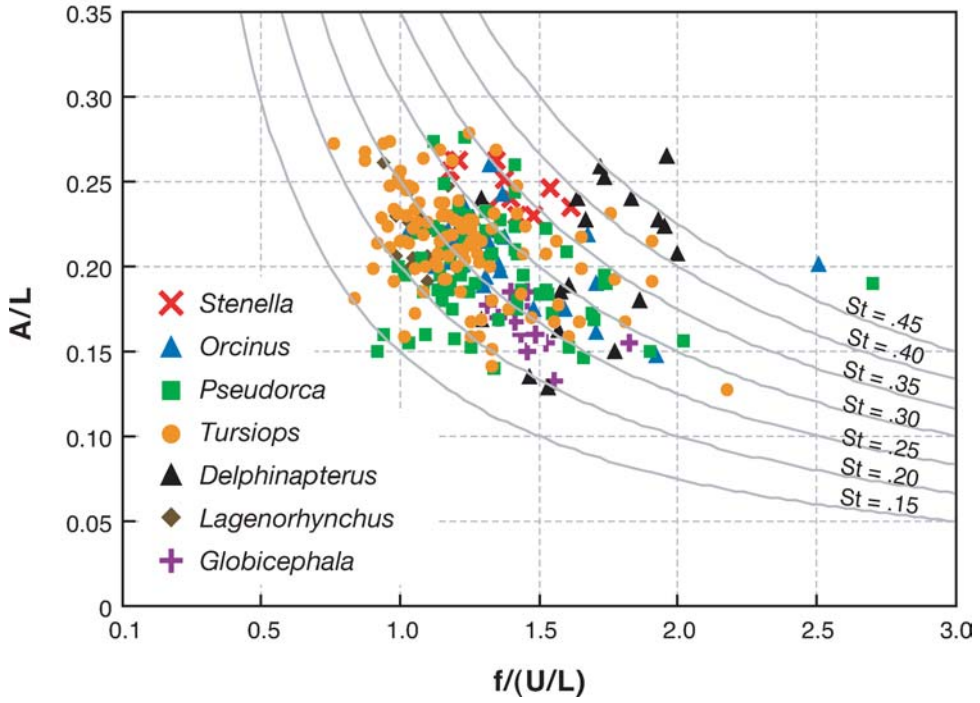

membrane that stretches between adjacent rays (Becerra et al. 1983, Lanzing 1976, Lauder 2005). In sharks these fin rays are cartilaginous and are single rod-like elements. However, in the 25,000 species of ray-finned fishes, fin rays have a remarkable bilaminar structure that has important implications for the hydrodynamic function of fins.

Each fin ray is composed of two halves, termed hemitrichs (Geerlink & Videler 1987, Lauder 2005), which are attached along their lengths and at the end by short ligaments and elastic fibers. Four separate muscles usually attach to the basal end of each ray, giving fish considerable control over fin ray position. If this musculature displaces one half of the ray to a greater extent than the other half, then the ray will curve, and control of curvature in this manner can be replicated in isolated fin rays. Bony fish thus have the ability to actively control the curvature of their control surfaces, a remarkable capability that makes fish propulsive surfaces different in character from insect wings and bird feathers (Lauder 2005). As a result, fish can actively resist hydrodynamic loading on the fin and curve their fin surfaces into oncoming flows.

3.4. Vorticity Production by Fish Fins

Only recently has high-resolution video data on the function of fins in freely swimming fishes executing various normal behaviors revealed how flexible fish fins actually are: Conformation and area of the fin surface may change substantially during execution of an individual locomotor sequence, as speed changes, and as the fish turns and brakes. For example, **Figure 13** shows a variety of shapes taken by the pectoral and dorsal fins of three species of fishes during locomotion. Individual fins such as the dorsal fin surface can achieve a bend of almost 90° during a maneuver, with little curvature of individual rays (**Figure 13*d***; Standen & Lauder 2005).

DPIV on the fins of freely swimming fishes has revealed a number of interesting hydrodynamic aspects of fin function. The most complete data set has been obtained on bluegill sunfish, for which experimental fluid dynamic data exist on fins during steady swimming at a range of speeds from 0.5 to 1.5 Ls^{-1}, maneuvering locomotion

Figure 12

Propulsive efficiency of cetaceans as a function of Strouhal number (*St*) (*top*). Colors indicate particular species: bottlenose dolphin, *Tursiops truncatus* (*orange*); false killer whale, *Pseudorca crassidens* (*green*); killer whale, *Orcinus orca* (*blue*); and beluga whale, *Delphinapterus leucas* (*black*). Nondimensional fluke-beat amplitude, *A/L*, as a function of nondimensional fluke-beat frequency, $f/(U/L)$, where A is the maximum excursion of the flukes, L is the body length, f is the fluke-beat frequency, and U is the swimming speed. Contours of constant Strouhal number, *St*, are included. Symbols indicate particular species: bottlenose dolphin, *Tursiops truncatus* (*solid orange circles*); false killer whale, *Pseudorca crassidens* (*closed green squares*); killer whale, *Orcinus orca* (*solid blue triangles*); and pilot whale, *Globicephala melaena* (*purple crosses*); Pacific striped dolphin, *Lagenorhynchus obliquidens* (*solid brown diamonds*); spotted dolphin, *Stenella frontalis* (*red crosses*); and beluga whale, *Delphinapterus leucas* (*solid black triangles*). From Rohr & Fish (2004).

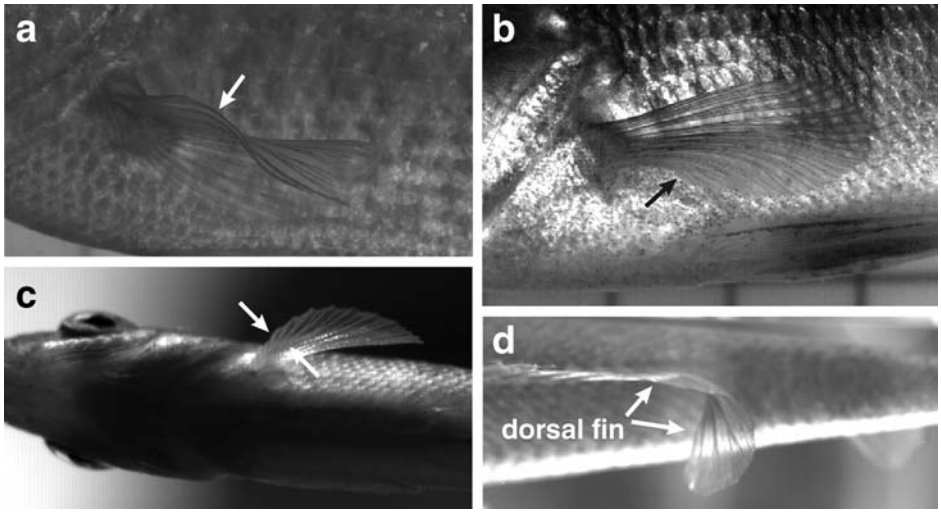

Figure 13

Sample images from high-speed videos of fish fin function showing the considerable flexibility of both individual fin rays and the entire fin. (*a*) Bluegill sunfish pectoral fin conformation during steady swimming. Arrow points to the wave of bending that travels from base to tip of the upper fin rays. (*b*) Pectoral fin maneuvering in yellow perch, *Perca flavescens*. Note how the lower (ventral) edge of the fin (*black arrow*) leads the rest of the fin out from the body. (*c*) Pectoral fin conformation during steady swimming in killifish, *Fundulus*. Both upper and lower fin edges (*arrows*) lead the middle of the fin as it moves away from the body. (*d*) Dorsal fin conformation during maneuvering in bluegill sunfish. Note that the whole fin is bent into almost a 90° angle but that individual fin rays are relatively straight (Panel *d* modified from Standen & Lauder 2005.)

and dorsal and anal fin function during both propulsion and maneuvering. **Figure 14** shows representative experimental hydrodynamic data from the bluegill pectoral fin (Drucker & Lauder 1999). DPIV in three separate orthogonal planes of sunfish swimming at 0.5 Ls^{-1} reveals that each plane shows formation of a single vortex. Bluegill sunfish swimming at 0.5 Ls^{-1} use only their pectoral fins for propulsion and there is a pause between each fin beat during which vorticity is shed from the fin. Significant downstream momentum is added to the flow as the fin moves out (away) from the body (**Figure 14*d***, frontal plane), indicating that thrust is generated by pectoral fins during both out and back fin movements. A schematic reconstruction of the vortex wake by sunfish swimming at 0.5 Ls^{-1} is shown in **Figure 15*a***, where the single fin forces estimated from the vortex wake are given (Drucker & Lauder 1999). As speed swimming speed increases, the formation of pectoral vortex rings changes and additional vorticity is shed on the upstroke (**Figure 15*b***), producing two rings, one of which remains attached to the body until it drifts back and is shed as a second ring.

In addition, differences in vortex wake structure are found among species and as swimming speed changes, which may partially explain why fish have gait transitions.

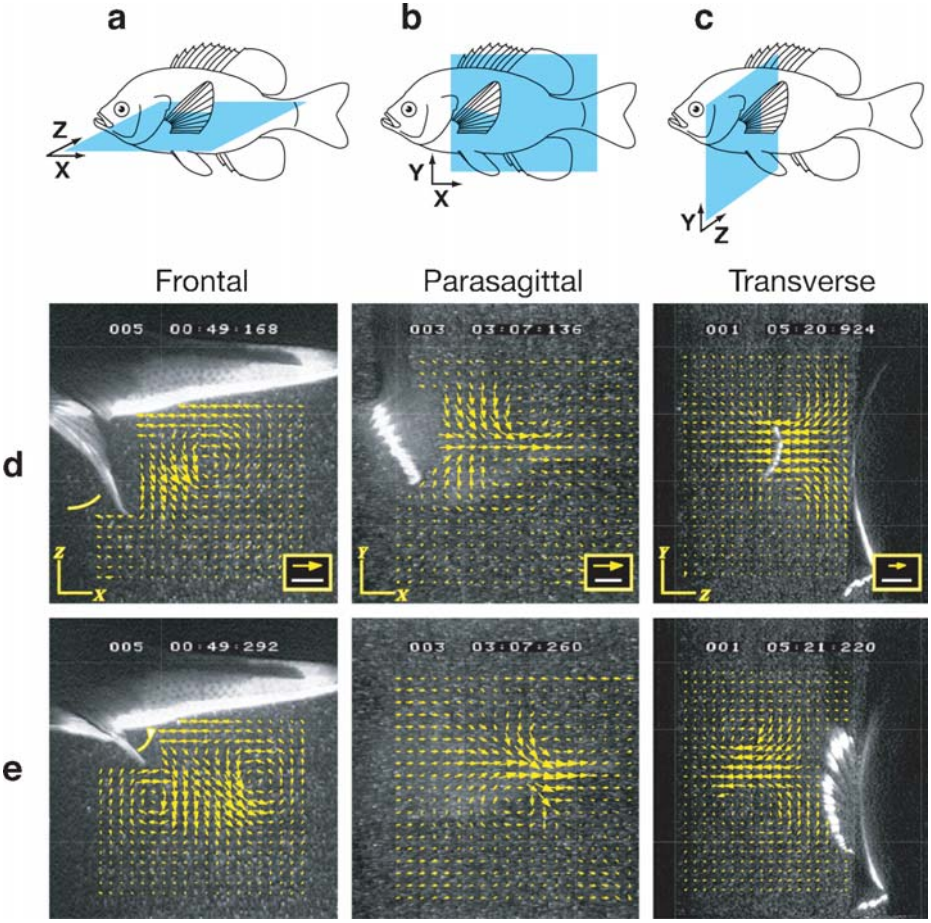

Figure 14

Experimental hydrodynamic data on fluid flows induced by the pectoral fin in freely swimming bluegill sunfish at 0.5 Ls^{-1}. Pectoral fin particle image velocimetry data obtained in separate experiments from three separate orthogonal planes (shown above) are illustrated. In the frontal and parasagittal planes (*a* and *b*), flow is from left to right; in the transverse plane (*c*), flow is from behind and out of the page in the vector plot below. Fluid flow patterns are shown for two times during the fin beat: The first row of plots (*d*) indicates flow at the time of fin beat reversal, the transition from movement out to movement toward the body. The lower three panels (*e*) show flow during the mid-to-late upstroke. The mean free-stream velocity of 10.5 cm s^{-1} was subtracted from all vectors in the frontal and parasagittal planes. Yellow arrow = 20 cm s^{-1}; bar = 1 cm. (Modified from Drucker & Lauder 1999.)

Bluegill sunfish use only their pectoral fins to generate locomotor force over a speed range of 0.5 Ls^{-1} to 1.1 Ls^{-1}, and above this speed they recruit additional fins to generate propulsive force (Drucker & Lauder 2000). Why do bluegill change gaits by adding the tail and dorsal and anal fins as thrust generators? Surfperch (*Embiotoca jacksoni*) continue to use their pectoral fins throughout a wide range of swimming speeds,

from 0.5 Ls^{-1} to 3.0 Ls^{-1}, and generate a double-linked vortex ring throughout this speed range without recruiting any additional fins (**Figure 15*c***). But as speed increases they reorient the vortex rings so that the central momentum jet is pointing directly downstream, with no side momentum (**Figure 15*d***). In contrast, as swimming speed increases in sunfish, pectoral fin vortex rings become increasingly oriented to

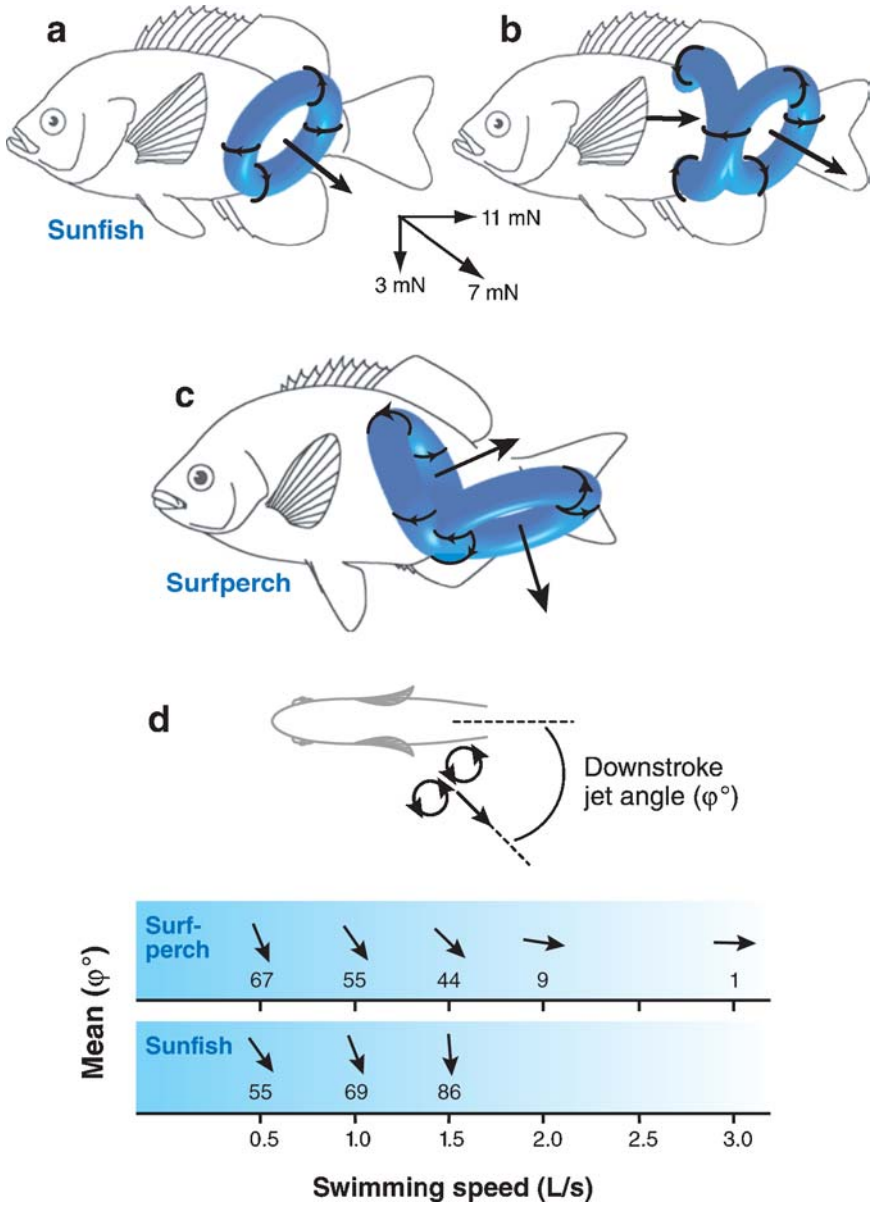

the side, so that less momentum is transferred to the water in a direction that would counter increasing drag forces (**Figure 15*d***). Bluegill rotate pectoral vortex rings to the side as speed increases, a direction that may enhance stability but not thrust. Other fins must then be recruited to accomplish a speed increase.

During yawing maneuvers, there is considerable functional differentiation between the right and left fins, and vortex rings from these fins are reoriented differently to accomplish the maneuver (Drucker & Lauder 2001b, 2002b, 2003). The diversity of hydrodynamic function in pectoral fins has also been studied during braking behaviors and across species (Drucker & Lauder 2002a,b, 2003; Wilga & Lauder 1999, 2000, 2001).

Dorsal and anal fins of fishes have often been ignored as contributors to locomotor dynamics due to a primary focus in the literature on the body and tail. These fins, however, contribute significantly to the generation of stabilizing forces and thrust, and greatly alter incident tail flow. The upper and lower lobes of the tail in fishes thus do not receive free-stream flow. Rather, they see incoming flow greatly altered as a result of active movement of the dorsal and anal fins (Drucker & Lauder 2001a, Lauder 2005, Lauder & Drucker 2004). Almost all fishes have a soft dorsal fin supported by flexible fin rays that can be actively moved by basal muscles (**Figure 16*a***, shaded fin) (Jayne et al. 1996, Winterbottom 1974). But many species also possess a distinct spiny portion that appears to stiffen the leading edge of the soft dorsal fin (**Figure 16*b***); the spiny dorsal fin is erected during rapid maneuvers, but remains depressed during routine steady swimming.

Representative vortex wakes shed by the dorsal fins of trout and sunfish are shown in **Figure 16*c*,*d***. In trout, the dorsal fin vortex wake at slower speeds consists of a series of alternating side jets with a linear array of vortex centers that reflects active oscillation of the dorsal fin. The tail traces an oscillatory path through these jets and passes through the vortex centers (**Figure 16*c***). At higher speeds (2.0 Ls^{-1} and greater) the dorsal fin is not actively moved and only a thin vortex sheet trails behind the fin. The strong sideways momentum generated by the dorsal fin is mirrored by the anal fin, which similarly produces side flows. Thus, trout, even when performing steady rectilinear locomotion, actively use both the dorsal and anal fins to generate stabilizing side forces.

Figure 15

(*a*, *b*) Schematic representation of the pectoral fin vortex wake in bluegill sunfish swimming at 0.5 and 1.0 Ls^{-1}, respectively. Mean stroke-averaged forces, calculated from the vortex wake, exerted by the pectoral fins during swimming at 0.5 Ls^{-1} are shown below these panels. The thrust force of 11 mN and the 3-mN lift force reflect thrust generated by both pectoral fins together, whereas the 7-mN side force is generated by each fin alone. (*c*) Pectoral fin vortex wake in surfperch at 1.0 Ls^{-1}. (*d*) Comparison of vortex ring momentum jet angle as speed increases in sunfish and surfperch. Note that in sunfish, the vortex rings rotate to the side as speed increases, necessitating the recruitment of additional fins to overcome drag. In surfperch, vortex rings rotate downstream, providing additional thrust and allowing surfperch to achieve much higher swimming speeds with their pectoral fins alone. (Modified from Drucker & Lauder 1999, 2000.)

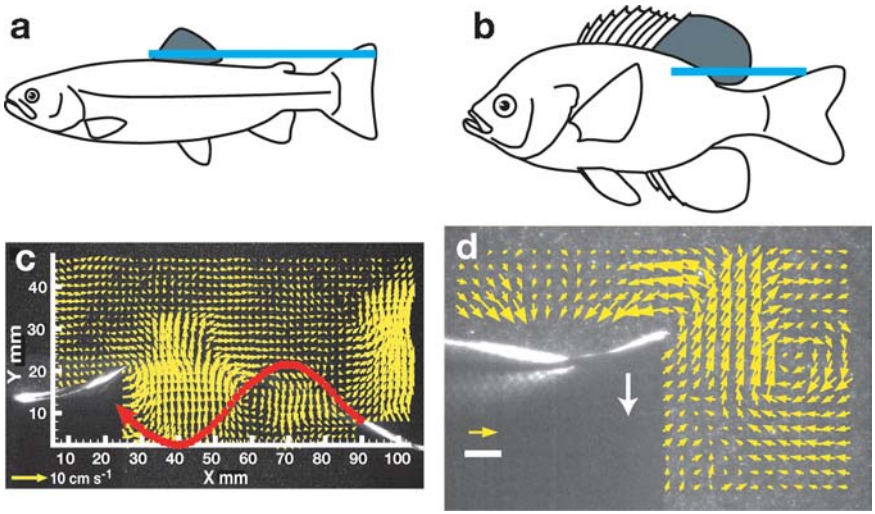

Figure 16

(*a*, *b*) Images of trout and bluegill (with the soft dorsal fin shaded) show the location of the laser light sheet (*blue line*) used to image flow between the dorsal fin and tail. Bluegill possess a distinct spiny dorsal fin located in front of the soft dorsal. (*c*, *d*) Dorsal fin particle image velocimetry wakes in trout and bluegill. Images were obtained from above, looking down on the wake shed by the soft dorsal fin. Red path in *c* shows the path of the tail of trout through the dorsal fin vortex wake. In trout, the dorsal fin generates a side wake with little downstream momentum, whereas in bluegill the dorsal fin produces considerable added momentum in the free-stream direction. (Modified from Drucker & Lauder 2001a, Lauder & Drucker 2004.)

3.5. Function of Mammal Flukes

Cetaceans (i.e., whale, dolphin, porpoise), which swim at high speeds, have a design encompassing high aspect ratio, oscillatory propulsors. Swimming is a highly derived locomotor behavior for mammals in which the caudal flukes act as hydrofoils to generate thrust by producing a lift force.

The hydrodynamic models that, in the past, were used to estimate thrust production and efficiency considered cetacean flukes as rigid hydrofoils or flat plates (Fish 1998a). However, the flukes can be bent along the axes of the chord (i.e., distance from leading to trailing edges) and span. Structurally, the flukes are lateral extensions from the tail, and although the central axis of the tail is supported by a series of bony caudal vertebrae (**Figure 17**), there are no bony supports in the fluke blades. The white-sided dolphin (*Lagenorhynchus acutus*) shows 35% deflection across the chord (Fish & Rohr 1999).

Flexibility across the chord can increase propulsive efficiency (Bose 1995, Katz & Weihs 1978). The efficiency of an oscillating, flexible hydrofoil is increased by 20% with a small decrease in thrust, compared to a rigid propulsor executing similar movements (Katz & Weihs 1978). In addition, bending across the chord throughout the stroke provides camber to the flukes (**Figure 17**). Cambering could change flow over the fluke surface to increase the forces generated. Cambering would be beneficial

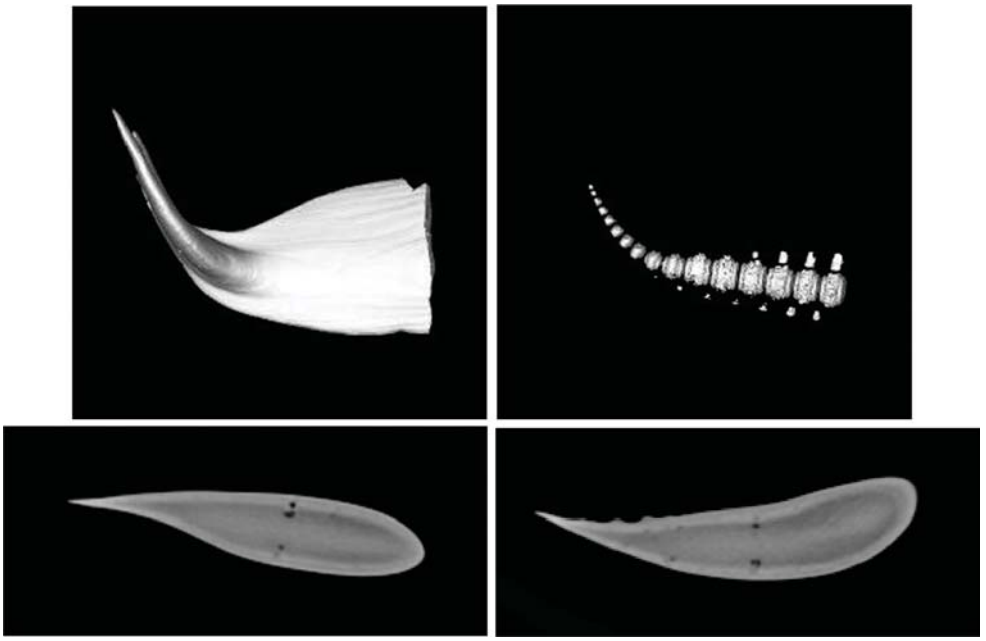

Figure 17

Computer Assisted Tomography (CAT scan) images from bent fluke of a bottlenose dolphin (*Tursiops truncatus*). A three-dimensional reconstruction of the flukes are shown in the top left. The vertebrae supporting the flukes in the tail are shown in the top right. Maximal bending occurs at the position of the "ball vertebra," which is located posterior of the anterior insertion of the flukes on the body. The lower images show cross sections through the fluke near 10% of span from the central axis of the body. The cross section on the left is for a relaxed, unbent fluke. The cross section on the right is for a fluke that is statically bent, showing cambering.

to maintain lift production at the end of each stroke as the propulsor changes direction, when there is a period of feathering (i.e., parallel to the incident flow, producing no thrust and reducing efficiency). The propulsive efficiency of cetacean flukes remains high compared to standard marine propellers (**Figure 18**).

3.6. Using Environmental Vortices

Aquatic animals often travel in highly organized formations. Some of these behaviors have been hypothesized to reduce drag and enhance locomotor performance of individuals (Fish 1999).

For animals, formation swimmers influence the flow of water around adjacent individuals. Vortices generated by anterior individuals pass backward and impact trailing individuals. If a trailing animal is oriented parallel and moving in the same direction to the tangential velocity of the vortex, the body will experience a reduction in its relative velocity. This reduction can decrease drag and the associated energy expenditure. Vorticity is shed into the wake of a passive body as two rows of

Figure 18

Comparison of relationships of propulsive efficiency and thrust coefficient for four species of small whales and a typical marine propeller. Data for the whales were obtained from Fish (1998), and data for the propeller (EMB 2294) are from Saunders (1957).

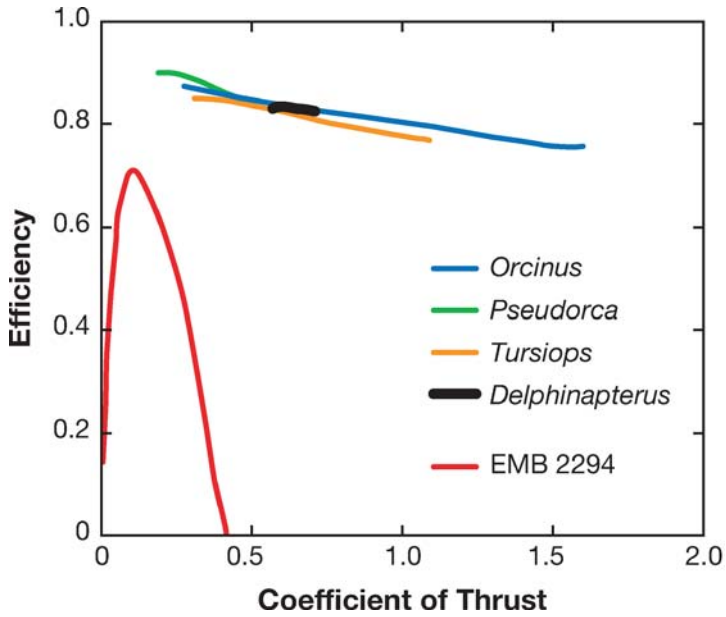

counter-rotating vortices (i.e., Kármán vortex street) where the optimal position for drag reduction is directly behind another body (Fish 1994). Although similar in pattern to the Kármán vortex street, a thrust-type vortex system has the opposite rotation of the vortices. In this system, which is generated by an oscillating foil, the optimal position is diagonal in a diamond pattern (Weihs 1973).

Thrust-type vortices produced by fish provide drag reduction in diamond-shaped formations (Weihs 1973). Trailing fish experience a relative velocity 40–50% of the free-stream velocity and a reduction of the force generated for swimming by a factor of 4 to 6. However, the decrease in relative velocity is not maintained with each successive row of trailing fish due to destructive interference.

Small whales often position themselves beside and slightly behind the maximum diameter of a larger animal (Weihs 2004). Whereas the larger whale experiences increased drag, the smaller individual gains an energetic benefit (Lang 1966). This effect is beneficial particularly for young whales in order to maintain speed with their mothers. A neonate can gain up to 90% of the thrust needed to move alongside the mother at swimming speeds up to 2.4 m/s (Weihs 2004).

A new locomotor behavior was recently described in which fishes can use vortices shed by objects in flowing water and radically alter their locomotor kinematics to maintain station well downstream of any suction region (Liao 2004; Liao et al. 2003a,b). This locomotor gait, termed the Kármán gait, was observed in fishes swimming 3 to 6 fish body lengths downstream of a cylindrical object in the Kármán vortex street shed by this object. When trout, for example, swim in a Kármán street, body kinematics are altered and large lateral oscillations of the center of mass occur as the body is buffeted from side to side in the vortex street. The amplitude of lateral

body movement and body curvature are both much greater than during free-stream locomotion (Liao et al. 2003b). Trout can maintain position in the central downstream flow in between vortices with very little activity of body musculature. This reduction in muscle activity when swimming in a Kármán vortex street strongly suggests that fishes are experiencing a considerable energy savings compared to free-stream locomotion.

4. PROSPECTUS

New insights into aquatic propulsion by animals can be exploited for the development of advanced propulsive technologies. These insights will come primarily from understanding the unsteady nature of animal movement, measurement of complex movement in three dimensions, use of computational methods that model both the animal's movement and its effect on the surrounding fluid, physiological and biomechanical studies of locomotor tissues in relation to thrust production and energy recycling, and analysis of appendages for thrust production, maneuvering, and stability.

ACKNOWLEDGMENTS

We appreciate the use of illustrations from L. Howle, E. Paterson, J. Rohr, J. Liao, and W. Rossiter. The research reported herein was supported in part by grants from the National Science Foundation, DARPA, and the Office of Naval Research. We are grateful to R. Mittal, P. Bandyopadhyay, E. Drucker, and P. Madden for numerous discussions related to the fluid dynamics of animal propulsion.

LITERATURE CITED

Aleyev YG. 1977. *Nekton*. The Hague: Junk

Anderson EJ, MacGillivray PS, DeMont ME. 1997. Scallop shells exhibit optimization of riblet dimensions for drag reduction. *Biol. Bull.* 192:341–44

Anderson EJ, McGillis W, Grosenbaugh MA. 2001. The boundary layer of swimming fish. *J. Exp. Biol.* 204:81–102

Anderson JM, Streitlien K, Barrett DS, Triantafyllou MS. 1998. Oscillating foils of high propulsive efficiency. *J. Fluid Mech.* 360:41–72

Askew GN, Marsh RL. 1997. The effects of length trajectory on the mechanical power output of mouse skeletal muscles. *J. Exp. Biol.* 200:3119–31

Bainbridge R. 1963. Caudal fin and body movement in the propulsion of some fish. *J. Exp. Biol.* 40:23–56

Bandyopadhyay PR. 2004. Biology-inspired science and technology for autonomous underwater vehicles. *IEEE J. Oceanic Eng.* 29:542–46

Bearman PW, Owen JC. 1998. Reduction of bluff-body drag and suppression of vortex shedding by the introduction of wavy separation lines. *J. Fluid Struct.* 12:123–30

Becerra J, Montes GS, Bexiga SR, Junqueira LC. 1983. Structure of the tail fin in teleosts. *Cell Tissue Res.* 230:127–37

Blake RW. 1983. *Fish Locomotion*. Cambridge: Cambridge Univ. Press

Bose N. 1995. Performance of chordwise flexible oscillating propulsors using a time-domain panel method. *Int. Shipbuild. Progr*. 42:281–94

Bushnell DM, Moore KJ. 1991. Drag reduction in nature. *Annu. Rev. Fluid Mech*. 23:65–79

Carling JC, Williams TL, Bowtell G. 1998. Self-propelled anguilliform swimming: simultaneous solution of the two-dimensional Navier-Stokes equations and Newton's laws of motion. *J. Exp. Biol.* 201:3143–66

Carpenter PW, Davies C, Lucey AD. 2000. Hydrodynamics and compliant walls: Does the dolphin have a secret? *Curr. Sci*. 79:758–65

Choi H, Moin P, Kim J. 1993. Direct numerical simulation of turbulent flow over riblets. *J. Fluid Mech*. 255:503–39

Dickinson MH, Lehmann F-O, Sane SP. 1999. Wing rotation and the aerodynamic basis of insect flight. *Science* 284:1954–60

Drucker EG, Lauder GV. 1999. Locomotor forces on a swimming fish: three-dimensional vortex wake dynamics quantified using digital particle image velocimetry. *J. Exp. Biol.* 202:2393–412

Drucker EG, Lauder GV. 2000. A hydrodynamic analysis of fish swimming speed: wake structure and locomotor force in slow and fast labriform swimmers. *J. Exp. Biol.* 203:2379–93

Drucker EG, Lauder GV. 2001a. Locomotor function of the dorsal fin in teleost fishes: experimental analysis of wake forces in sunfish. *J. Exp. Biol.* 204:2943–58

Drucker EG, Lauder GV. 2001b. Wake dynamics and fluid forces of turning maneuvers in sunfish. *J. Exp. Biol.* 204:431–42

Drucker EG, Lauder GV. 2002a. Experimental hydrodynamics of fish locomotion: functional insights from wake visualization. *Int. Comp. Biol.* 42:243–57

Drucker EG, Lauder GV. 2002b. Wake dynamics and locomotor function in fishes: interpreting evolutionary patterns in pectoral fin design. *Int. Comp. Biol.* 42:997–1008

Drucker EG, Lauder GV. 2003. Function of pectoral fins in rainbow trout: behavioral repertoire and hydrodynamic forces. *J. Exp. Biol.* 206:813–26

Ellington CP, van den Berg C, Willmott AP, Thomas ALR. 1996. Leading-edge vortices in insect flight. *Nature* 384:626–30

Ferry LA, Lauder GV. 1996. Heterocercal tail function in leopard sharks: a three-dimensional kinematic analysis of two models. *J. Exp. Biol.* 199:2253–68

Fish FE. 2004. Structure and mechanics of nonpiscine control surfaces. *IEEE J. Oceanic Eng.* 29:605–21

Fish FE. 1993. Influence of hydrodynamic design and propulsive mode on mammalian swimming energetics. *Aust. J. Zool*. 42:79–101

Fish FE. 1994. Energy conservation by formation swimming: metabolic evidence from ducklings. In *Mechanics and Physiology of Animal Swimming*, ed. L Maddock, Q Bone, JMV Rayner, pp. 193–204. Cambridge: Cambridge Univ. Press. 250 pp.

Fish FE. 1998a. Biomechanical perspective on the origin of cetacean flukes. In *The Emergence of Whales: Evolutionary Patterns in the Origin of Cetacea*, ed. JGM Thewissen, pp. 303–24, New York: Plenum. 477 pp.
Fish FE. 1998b. Comparative kinematics and hydrodynamics of odontocete cetaceans: morphological and ecological correlates with swimming performance. *J. Exp. Biol.* 201:2867–77
Fish FE. 1999. Energetics of swimming and flying in formation. *Comm. Theor. Biol.* 5:283–304
Fish FE. 2000. Biomechanics and energetics in aquatic and semiaquatic mammals: platypus to whale. *Physiol. Biochem. Zool.* 73:683–98
Fish FE, Battle JM. 1995. Hydrodynamic design of the humpback whale flipper. *J. Morphol.* 225:51–60
Fish FE, Hui CA. 1991. Dolphin swimming—a review. *Mamm. Rev.* 21:181–95
Fish FE, Innes S, Ronald K. 1988. Kinematics and estimated thrust production of swimming harp and ringed seals. *J. Exp. Biol.* 137:157–73
Fish FE, Rohr J. 1999. Review of dolphin hydrodynamics and swimming performance. *Space Nav. Warf. Syst. Cent. Tech. Rep.* 1801
Fitzgerald JW. 1991. Artificial dolphin blubber could increase sub speed, cut noise. *Navy News Undersea Tech.* 9:1–2
Fitzgerald JW, Fitzgerald ER, Carey WM, von Winkle WA. 1995. Blubber and compliant coatings for drag reduction in water. II. Matched shear impedance for compliant layer drag reduction. *Mat. Sci. Eng. C* 2:215–20
Gad-el-Hak M. 1987. Compliant coatings research: a guide to the experimentalist. *J. Fluid. Struct.* 1:55–70
Geerlink PJ, Videler J. 1987. The relation between structure and bending properties of teleost fin rays. *Neth. J. Zool.* 37:59–80
Gibb AC, Dickson KA, Lauder GV. 1999. Tail kinematics of the chub mackerel *Scomber japonicus*: testing the homocercal tail model of fish propulsion. *J. Exp. Biol.* 202:2433–47
Gillis GB. 1996. Undulatory locomotion in elongate aquatic vertebrates: anguilliform swimming since Sir James Gray. *Am. Zool.* 36:656–65
Gillis GB. 1998. Environmental effects on undulatory locomotion in the American eel *Anguilla rostrata*: kinematics in water and on land. *J. Exp. Biol.* 201:949–61
Gopalkrishnan R, Triantafyllou MS, Triantafyllou GS, Barrett D. 1994. Active vorticity control in a shear flow using a flapping foil. *J. Fluid Mech.* 274:1–21
Gosline WA. 1971. *Functional Morphology and Classification of Teleostean Fishes*. Honolulu: Univ. Hawaii Press
Gray J. 1933. Studies in animal locomotion. I. The movement of fish with special reference to the eel. *J. Exp. Biol.* 10:88–104
Gray J. 1936. Studies in animal locomotion VI. The propulsive powers of the dolphin. *J. Exp. Biol.* 13:192–99
Gray J. 1968. *Animal Locomotion*. London: Weidenfeld and Nicolson
Haider M, Lindsley DB. 1964. Microvibrations in man and dolphin. *Science* 146:1181–83
Harrison RJ, Thurley KW. 1972. Fine structural features of delphinid epidermis. *J. Anat.* 111:498–99

Henderson Y, Haggard HW. 1925. The maximum of human power and its fuel. *Am. J. Physiol.* 72:264–82
Jayne BC, Lauder GV. 1994. How swimming fish use slow and fast muscle fibers: implications for models of vertebrate muscle recruitment. *J. Comp. Physiol. A* 175:123–31
Jayne BC, Lozada A, Lauder GV. 1996. Function of the dorsal fin in bluegill sunfish: motor patterns during four locomotor behaviors. *J. Morphol.* 228:307–26
Katz J, Weihs D. 1978. Hydrodynamic propulsion by large amplitude oscillation of an airfoil with chordwise flexibility. *J. Fluid Mech.* 88:485–97
Kayan VP. 1974. Resistance coefficient of the dolphin. *Bionika* 8:31–35 (From Russian)
Kramer MO. 1960a. Boundary layer stabilization by distributed damping. *J. Amer. Soc. Nav. Eng.* 72:25–33
Kramer MO. 1960b. The dolphins' secret. *New Sci.* 7:1118–20
Landahl MT. 1962. On stability of a laminar incompressible boundary layer over a flexible surface. *J. Fluid Mech.* 13:609–32
Lang TG. 1966. Hydrodynamic analysis of cetacean performance. In *Whales, Dolphins and Porpoises*, ed. KS Norris, pp. 410–32. Berkley, CA: Univ. California Press. 789 pp.
Lang TG, Daybell DA. 1963. Porpoise performance tests in a seawater tank. *Nav. Ord. Test Sta. Tech. Rep.* 3063
Lanzing WJR. 1976. The fine structure of fins and finrays of *Tilapia mossambica* (Peters). *Cell Tissue Res.* 173:349–56
Lauder GV. 1982. Structure and function of the caudal skeleton in the pumpkinseed sunfish, *Lepomis gibbosus*. *J. Zool. London* 197:483–95
Lauder GV. 1989. Caudal fin locomotion in ray-finned fishes: historical and functional analyses. *Am. Zool.* 29:85–102
Lauder GV. 2000. Function of the caudal fin during locomotion in fishes: kinematics, flow visualization, and evolutionary patterns. *Am. Zool.* 40:101–22
Lauder GV. 2005. Locomotion. In *The Physiology of Fishes, Third Edition*, ed. DH Evans, JB Claiborne, pp. 3–46. Boca Raton: CRC
Lauder GV, Drucker E. 2002. Forces, fishes, and fluids: hydrodynamic mechanisms of aquatic locomotion. *News Physiol. Sci.* 17:235–40
Lauder GV, Drucker EG. 2004. Morphology and experimental hydrodynamics of fish fin control surfaces. *IEEE J. Oceanic Eng.* 29:556–71
Lauder GV, Drucker EG, Nauen J, Wilga CD. 2003. Experimental hydrodynamics and evolution: caudal fin locomotion in fishes. In *Vertebrate Biomechanics and Evolution*, ed. V Bels, J-P Gasc, A Casinos, pp. 117–35. Oxford: Bios Sci. Publ.
Lauder GV, Long JH Jr. 1996. Aquatic locomotion: new approaches to invertebrate and vertebrate biomechanics. *Am. Zool.* 36:535–36
Lauder GV, Nauen J, Drucker EG. 2002. Experimental hydrodynamics and evolution: function of median fins in ray-finned fishes. *Int. Comp. Biol.* 42:1009–17
Lauder GV, Tytell ED. 2004. Three Gray classics on the biomechanics of animal movement. *J. Exp. Biol.* 207:1597–99
Liao J. 2004. Neuromuscular control of trout swimming in a vortex street: implications for energy economy during the Kármán gait. *J. Exp. Biol.* 207:3495–506

Liao J, Beal DN, Lauder GV, Triantafyllou MS. 2003a. Fish exploiting vortices decrease muscle activity. *Science* 302:1566–69

Liao J, Beal DN, Lauder GV, Triantafyllou MS. 2003b. The Kármán gait: novel body kinematics of rainbow trout swimming in a vortex street. *J. Exp. Biol.* 206:1059–73

Liao J, Lauder GV. 2000. Function of the heterocercal tail in white sturgeon: flow visualization during steady swimming and vertical maneuvering. *J. Exp. Biol.* 203:3585–94

Lighthill J. 1960. Note on the swimming of slender fish. *J. Fluid Mech.* 9:305–17

Lighthill J. 1971. Large-amplitude elongated body theory of fish locomotion. *Proc. R. Soc. London Ser. B* 179:125–38

Liu H, Wassersug RJ, Kawachi K. 1997. The three-dimensional hydrodynamics of tadpole locomotion. *J. Exp. Biol.* 200:2807–19

McCutchen CW. 1977. Froude propulsive efficiency of a small fish, measured by wake visualization. In *Scale Effects in Animal Locomotion*, ed. TJ Pedley, pp. 339–63. London: Academic. 545 pp.

Miklosovic DS, Murray MM, Howle LE, Fish FE. 2004. Leading edge tubercles delay stall on humpback whale (*Megaptera novaeangliae*) flippers. *Phys. Fluids* 16:L39–L42

Moin P, Kim J. 1997. Tackling turbulence with supercomputers. *Sci. Am.* 276:62–68

Muller U, Smit J, Stamhuis E, Videler J. 2001. How the body contributes to the wake in undulatory fish swimming: flow fields of a swimming eel (*Anguilla anguilla*). *J. Exp. Biol.* 204:2751–62

Müller UK, Stamhuis EJ, Videler JJ. 2000. Hydrodynamics of unsteady fish swimming and the effects of body size: comparing the flow fields of fish larvae and adults. *J. Exp. Biol.* 203:193–206

Muller UK, Van den Heuvel B, Stamhuis EJ, Videler JJ. 1997. Fish foot prints: morphology and energetics of the wake behind a continuously swimming mullet (*Chelon labrosus* Risso). *J. Exp. Biol.* 200:2893–906

Nagamine H, Yamahata K, Hagiwara Y, Matsubara R. 2004. Turbulence modification by compliant skin and strata-corneas desquamation of a swimming dolphin. *J. Turbulence* 5:1–25

Nauen JC, Lauder GV. 2000. Locomotion in scombrid fishes: morphology and kinematics of the finlets of the Chub mackerel *Scomber japonicus*. *J. Exp. Biol.* 203:2247–59

Nauen JC, Lauder GV. 2001a. Locomotion in scombrid fishes: visualization of flow around the caudal peduncle and finlets of the Chub mackerel *Scomber japonicus*. *J. Exp. Biol.* 204:2251–63

Nauen JC, Lauder GV. 2001b. Three-dimensional analysis of finlet kinematics in the Chub mackerel (*Scomber japonicus*). *Biol. Bull.* 200:9–19

Nauen JC, Lauder GV. 2002a. Hydrodynamics of caudal fin locomotion by chub mackerel, *Scomber japonicus* (Scombridae). *J. Exp. Biol.* 205:1709–24

Nauen JC, Lauder GV. 2002b. Quantification of the wake of rainbow trout (*Oncorhynchus mykiss*) using three-dimensional stereoscopic digital particle image velocimetry. *J. Exp. Biol.* 205:3271–79

Owen JC, Szewezyk AA, Bearman PW. 2000. Suppression of karman vortex shedding, Gallery of Fluid Motion. *Phys. Fluids* 12:1–13
Paterson EG, Wilson RV, Stern F. 2003. General-purpose parallel unsteady RANS CFD code for ship hydrodynamics. *IIHR Hydrosci. Eng. Rep. 531*, Univ. Iowa, Iowa City, Iowa
Ramamurti R, Sandberg WC, Lohner R, Walker JA, Westneat M. 2002. Fluid dynamics of flapping aquatic flight in the bird wrasse: three-dimensional unsteady computations with fin deformation. *J. Exp. Biol.* 205:2997–3008
Rayner JMV. 1985. Vorticity and propulsion mechanics in swimming and flying animals. In *Konstruktionsprinzipen Lebender und Ausgestorbener Reptilien*, ed. J Riess, E Frey, pp. 89–118. Tubingen, FRG: Univ. Tubingen
Reif W-E. 1978. Protective and hydrodynamic function of the dermal skeleton of elasmobranchs. *Neues Jahrb. Geol. Paläotol.* 157:133–41
Reif W-E, Dinkelacker A. 1982. Hydrodynamics of the squamation in fast swimming sharks. *Neues Jahrb. Geol. Paläotol.* 164:184–87
Ridgway SH, Carder DA. 1993. Features of dolphin skin with potential hydrodynamic importance. *IEEE Eng. Med. Biol.* 12:83–88
Riley JJ, Gad-el-Hak M, Metcalfe RW. 1988. Compliant coatings. *Annu. Rev. Fluid Mech.* 20:393–420
Rohr J, Latz MI, Fallon S, Nauen JC, Hendricks E. 1998. Experimental approaches towards interpreting dolphin-stimulated bioluminescence. *J. Exp. Biol.* 201:1447–60
Rohr JJ, Fish FE. 2004. Strouhal numbers and optimization of swimming by odontocete cetaceans. *J. Exp. Biol.* 207:1633–42
Romanenko EV. 1995. Swimming of dolphins: experiments and modelling. In *Biological Fluid Dynamics*, ed. CP Ellington, TJ Pedley, pp. 21–33. Cambridge, UK: Co. Biol. 363 pp.
Romanenko EV, Yanov VG. 1973. Experimental results of studying the hydrodynamics of dolphins. *Bionika* 7:52–56 (From Russian)
Saunders HE. 1957. *Hydrodynamics of Ship Design*. New York: Soc. Nav. Arch. Mar. Eng.
Sokolov V, Bulina I, Rodionov V. 1969. Interaction of dolphin epidermis with flow boundary layer. *Nature* 222:267–68
Standen EM, Lauder GV. 2005. Dorsal and anal fin function in bluegill sunfish (*Lepomis macrochirus*): three-dimensional kinematics during propulsion and maneuvering. *J. Exp. Biol.* 205:2753–63
Triantafyllou GS, Triantafyllou MS. 1995. An efficient swimming machine. *Sci. Am.* 272:40–48
Triantafyllou MS, Techet AH, Hover FS. 2004. Review of experimental work in biomimetic foils. *IEEE J. Oceanic Eng.* 29:585–94
Triantafyllou MS, Triantafyllou GS, Gopalkrishnan R. 1991. Wake mechanics for thrust generation in oscillating foils. *Phys. Fluids* 3:2835–37
Triantafyllou MS, Triantafyllou GS, Yue DKP. 2000. Hydrodynamics of fishlike swimming. *Annu. Rev. Fluid Mech.* 32:33–53
Tytell ED. 2004a. The hydrodynamics of eel swimming II. Effect of swimming speed. *J. Exp. Biol.* 207:3265–79

Tytell ED. 2004b. Kinematics and hydrodynamics of linear acceleration in eels, *Anguilla rostrata*. *Proc. R. Soc. London Ser. B* 271:2535–40
Tytell ED, Lauder GV. 2004. The hydrodynamics of eel swimming. I. Wake structure. *J. Exp. Biol.* 207:1825–41
Uskova Ye T, Shmyrev AN, Rayevskiy VS, Bogdanova LN, Momot LN, et al. 1983. The nature and hydrodynamic activity of dolphin eye secretions. *Bionika* 17:72–75 (From Russian)
Walsh MJ. 1990. Riblets. *Prog. Astro. Aero*. 123:203–61
Watts P, Fish FE. 2001. The influence of passive, leading edge tubercles on wing performance. In *Proc. Twelfth Intl. Symp. Unmanned Untethered Submers. Technol*. Durham New Hampshire: Auton. Undersea Syst. Inst.
Webb PW. 1975. Hydrodynamics and energetics of fish propulsion. *Bull. Fish Res. Bd. Can.* 190:1–159
Webb PW. 1998. Swimming. In *The Physiology of Fishes, 2nd edition*, ed. DH Evans, pp. 3–24. Boca Raton, Florida: CRC
Webster DR, Longmire EK. 1997. Vortex dynamics in jets from inclined nozzles. *Phys. Fluids* 9:655–66
Webster DR, Longmire EK. 1998. Vortex rings from cylinders with inclined exits. *Phys. Fluids* 10:400–16
Weihs D. 1972a. A hydrodynamic analysis of fish turning manoeuvres. *Proc. R. Soc. London Ser. B* 182B:59–72
Weihs D. 1972b. Semi-infinite vortex trails, and their relation to oscillating airfoils. *J. Fluid Mech.* 54:679–90
Weihs D. 1973. Hydromechanics of fish schooling. *Nature* 241:290–91
Weihs D. 1993. Stability of aquatic animal locomotion. *Cont. Math*. 141:443–61
Weihs D. 2004. The hydrodynamics of dolphin drafting. *J. Biol.* 3:1–16
Wilga CD, Lauder GV. 2004a. Biomechanics of locomotion in sharks, rays and chimeras. In *Biology of Sharks and Their Relatives*, ed. JC Carrier, JA Musick, MR Heithaus, pp. 139–64. Boca Raton: CRC
Wilga CD, Lauder GV. 1999. Locomotion in sturgeon: function of the pectoral fins. *J. Exp. Biol.* 202:2413–32
Wilga CD, Lauder GV. 2000. Three-dimensional kinematics and wake structure of the pectoral fins during locomotion in leopard sharks *Triakis semifasciata*. *J. Exp. Biol.* 203:2261–78
Wilga CD, Lauder GV. 2001. Functional morphology of the pectoral fins in bamboo sharks, *Chiloscyllium plagiosum*: benthic versus pelagic station holding. *J. Morphol.* 249:195–209
Wilga CD, Lauder GV. 2004b. Hydrodynamic function of the shark's tail. *Nature* 430:850
Williams TM, Davis RW, Fuiman LA, Francis J, LeBoeuf BJ, et al. 2000. Sink or swim: strategies for cost-efficient diving by marine mammals. *Science* 288:133–36
Williams TM, Friedl WA, Fong ML, Yamada RM, Sedivy P, Haun JE. 1992. Travel at low energetic cost by swimming and wave-riding bottlenose dolphins. *Nature* 355:821–23

Winterbottom R. 1974. A descriptive synonymy of the striated muscles of the Teleostei. *Proc. Acad. Nat. Sci. Philos.* 125:225–317

Wolfgang MJ, Anderson JM, Grosenbaugh M, Yue D, Triantafyllou M. 1999. Near-body flow dynamics in swimming fish. *J. Exp. Biol.* 202:2303–27

Wood FG. 1973. *Marine Mammals and Man: The Navy's Porpoises and Sea Lions*. Washington: Robert B. Luce

Yurchenko NF, Babenko VV. 1980. Stabilization of the longitudinal vortices by skin integuments of dolphins. *Biophysics* 25:309–15

Zangerl R, Case GR. 1973. Iniopterygia, a new order of chondrichthyan fishes from the Pennsylvanian of North America. *Fieldiana Geol. Mem*. 6:1–67